Materials Today Bio 25 (2024) 100990

Contents lists available at ScienceDirect

Materials Today Bio

journal homepage: www.journals.elsevier.com/materials-today-bio

Molecular insights into the proteomic composition of porcine treated dentin matrix

Xiya Zhang [a,b,c,1], Sha Zhou [a,b,c,1], Yuzhen Zhan [a,b,c,1], Ziyi Mei [a,b,c], Aizhuo Qian [a,b,c], Yu Yuan [a,b,c], Xiaonan Zhang [a,b,c], Tiwei Fu [a,b,c], Shiyong Ma [d,**], Jie Li [a,b,c,*]

[a] College of Stomatology, Chongqing Medical University, Chongqing, China
[b] Chongqing Key Laboratory of Oral Diseases and Biomedical Sciences, Chongqing Medical University, Chongqing, China
[c] Chongqing Municipal Key Laboratory of Oral Biomedical Engineering of Higher Education, Chongqing Medical University, Chongqing, China
[d] Basic Medicine Research and Innovation Center for Novel Target and Therapeutic Intervention, The Ministry of Education, Institute of Life Sciences, Chongqing Medical University, Chongqing, China

ARTICLE INFO

Keywords:
Extracellular matrix
Treated dentin matrix
Dentin-pulp regeneration
Proteomics
Stem cells from human exfoliated deciduous teeth

ABSTRACT

Background: Human-treated dentin matrix (hTDM) has recently been studied as a natural extracellular matrix-based biomaterial for dentin pulp regeneration. However, porcine-treated dentin matrix (pTDM) is a potential alternative scaffold due to limited availability. However, there is a dearth of information regarding the protein composition and underlying molecular mechanisms of pTDM.

Methods: hTDM and pTDM were fabricated using human and porcine teeth, respectively, and their morphological characteristics were examined using scanning electron microscopy. Stem cells derived from human exfoliated deciduous teeth (SHEDs) were isolated and characterized using flow cytometry and multilineage differentiation assays. SHEDs were cultured in three-dimensional environments with hTDM, pTDM, or biphasic hydroxyapatite/tricalcium phosphate. The expression of odontogenesis markers in SHEDs were assessed using real-time polymerase chain reaction and immunochemical staining. Subsequently, SHEDs/TDM and SHEDs/HA/TCP complexes were transplanted subcutaneously into nude mice. The protein composition of pTDM was analyzed using proteomics and compared to previously published data on hTDM.

Results: pTDM and hTDM elicited comparable upregulation of odontogenesis-related genes and proteins in SHEDs. Furthermore, both demonstrated the capacity to stimulate root-related tissue regeneration *in vivo*. Proteomic analysis revealed the presence of 278 protein groups in pTDM, with collagens being the most abundant. Additionally, pTDM and hTDM shared 58 identical proteins, which may contribute to their similar abilities to induce odontogenesis.

Conclusions: Both hTDM and pTDM exhibit comparable capabilities in inducing odontogenesis, potentially owing to their distinctive bioactive molecular networks.

1. Introduction

The extracellular matrix (ECM) is a non-cellular, three-dimensional (3D) macromolecular network in all tissues and organs. Its structural constituents comprise collagen, elastin, fibronectin, lamellae, proteoglycans/glycosaminoglycans, and other glycoproteins [1,2]. ECM is extensively utilized in regenerative medicine as a scaffold material due to its inherent structural properties that facilitate tissue support and create a dynamic milieu for cellular reactions [3–7]. Tissue-derived ECM from various sources, such as the bladder, small intestine, heart, cartilage, skin, and tooth-related tissues, can be utilized [8–10]. Besides its inherent biocompatibility and resemblance to the mechanical configuration of homologous tissues, the principal benefit of employing ECM as a scaffold material is its ability to induce constructive remodeling [11,12]. During remodeling, there is significant infiltration of host cells, mitosis, angiogenesis, and deposition of new host ECM [11]. ECM has

* Corresponding author. College of Stomatology, Chongqing Medical University. 426# Songshibei Road, Yubei District, Chongqing, 401147, China.
** Corresponding author. Basic Medicine Research and Innovation Center for Novel Target and Therapeutic Intervention, The Ministry of Education, Institute of Life Sciences, Chongqing Medical University, 1# Yixueyuan Road, Yuzhong District, Chongqing, 400016, China.
E-mail addresses: shiyongma@cqmu.edu.cn (S. Ma), jieli@hospital.cqmu.edu.cn (J. Li).
[1] These authors contributed equally to this work.

https://doi.org/10.1016/j.mtbio.2024.100990
Received 7 November 2023; Received in revised form 23 January 2024; Accepted 3 February 2024
Available online 5 February 2024

the necessary characteristics to be an ideal scaffold material in tissue engineering, including favorable mechanical properties, non-degradability, and good biocompatibility.

A specific type of ECM scaffold derived from natural teeth, known as treated dentin matrix (TDM) [13–22], provides structural support and retains proteins and growth factors. Moreover, human TDM (hTDM) releases odontogenic proteins, such as dentin matrix protein 1 (DMP1) and dentin sialophosphoprotein (DSPP), thereby creating a natural odontogenic-inducing 3D environment [10,23]. Consequently, hTDM is a biologically active scaffold material with extensive applications in dentin-pulp regeneration [14,15,19,20] and periodontal regeneration [24]. Given the scarcity of human-derived teeth, it is crucial to investigate alternative sources of TDM. Xenotransplantation has emerged as a viable option due to the scarcity of organ transplant donors. Pigs have garnered attention in the quest for suitable animal donors due to their rapid growth and reproductive capabilities, abundant availability as donors, cost-effectiveness in maintenance, and organ sizes that closely resemble those of primates, rendering them more suitable candidates [25,26]. The morphological resemblance between porcine TDM (pTDM) and hTDM has garnered the attention of researchers.

Stem cells from human exfoliated deciduous teeth (SHED), derived from neural crest cells, are highly proliferative, clonogenic, and multipotent stem cells that can differentiate into osteoblasts, odontoblasts, and neural cells *in vitro* and *in vivo*. Previous studies have demonstrated that combining pTDM and SHED can stimulate bio-root regeneration [20]. However, the specific protein composition of pTDM has not been reported, and the underlying molecular mechanism responsible for pTDM-induced dentin-pulp tissue regeneration has not been elucidated. Furthermore, investigations have indicated that this xenogeneic TDM induces dentin-pulp tissue regeneration alongside immune responses [22], necessitating further exploration into the immunogens present in pTDM and the development of effective immune regulation methods.

This study primarily aimed to investigate the specific components of pTDM that exert odontogenic functions in dentin-pulp tissue construction. We proposed potential solutions for the limited availability of hTDM sources and immune responses associated with xenogeneic TDM. This study compared the structural characteristics of hTDM and pTDM. We evaluated the ability of hTDM and pTDM to induce odontogenic differentiation in SHEDs *in vitro* and *in vivo*. Additionally, we analyzed the protein composition of pTDM using the proteomic methods and compared it with hTDM to identify protein groups that can induce odontogenesis.

2. Materials and methods

2.1. Preparation of hTDM and pTDM

According to a previously reported method [15,16,19–21], healthy premolars or third molars extracted for clinical reasons were collected clinically, and deciduous incisors were obtained from pigs slaughtered in the morning. The periodontal tissue was completely scraped away with a curette, the outer cementum and part of the dentin were removed, and the dental pulp tissues and pre-dentin were mostly removed using a dental handpiece. The hTDM and pTDM formed cones with a diameter of approximately 3–5 mm and a length of approximately 6–7 mm. hTDM was treated as follows: 17% ethylenediaminetetraacetic acid (EDTA, Sigma-Aldrich, St. Louis, MO, USA) for 25 min, 10% EDTA for 25 min, and 5% EDTA for 25 min pTDM was treated with 17%, 10%, and 5% EDTA for 20 min. After each EDTA concentration, the samples were mechanically cleaned in deionized water using an ultrasonic cleaner for 10 min and stored in penicillin-streptomycin solution (HyClone, Logan, UT, USA) overnight at −80 °C. Hydroxyapatite/tricalcium phosphate (HA/TCP) scaffolds were purchased from Sichuan Baiamon Bioactive Materials Co. Ltd., Chengdu, China.

2.2. Chemical composition analysis

The prepared pTDM and hTDM were placed in a low-temperature freezing-grinding instrument (JXFSTPRP-CL; Shanghai, China). The temperature was set to −50 °C, and grinding was performed at 60 Hz/min for 1 min. After repeating this step three to five times, the obtained powder was TDM powder. The chemical properties of the hTDM and pTDM powders were examined using Fourier-transform infrared (FTIR) spectroscopy (Thermo Scientific Nicolet iS20). Infrared spectra were recorded in the wavelength range of 400–4000 cm^{-1} using a beam splitter coated with Ge on a KBr detector with a resolution of 4 cm^{-1} (with 32 scans). Raman analyses of pTDM and hTDM powders were performed using DXR3 Flex Raman Spectrometer (Thermo Scientific DXR3) coupled with a Peltier-cooled Charge Coupled Device (CCD) detector. Excitation was provided by the 785 nm line of the diode laser. Spectra were collected from 100 to 3500 cm^{-1} wavenumber shifts at a spectral resolution of 2 cm^{-1} using a 60 s integration time.

2.3. Cell culture

Previous studies have confirmed that SHEDs are a potential cell source for bio-root regeneration [14]. In this study, SHEDs were co-cultured with pTDM, hTDM, and HA/TCP to verify the odontogenesis-inducing ability of these two TDM *in vitro* and *in vivo*. Non-inflamed and carious deciduous teeth were collected from children aged 5−12. Informed consent was signed by the child's guardian. The dentin-pulp tissues were extracted from the exfoliated deciduous teeth, washed twice in sterile phosphate-buffered saline (PBS, Solarbio, Beijing, China), cut into 1 × 1 mm sections, and digested with 3% type I collagenase (Sigma-Aldrich, St. Louis, MO, USA) for 30 min. The digested tissues were cultured in α-minimum essential medium (α-MEM, HyClone, Logan, UT, USA) containing 10% fetal bovine serum (FBS; Gemini Bio-Products, Woodland, CA, USA) in a humidified incubator with 5% CO_2 at 37 °C.

2.4. Flow cytometry

The SHEDs were collected and digested into single cells using trypsin. According to the cell count result, 10^6 cells were added to each centrifuge tube. Antibodies including FITC-conjugated antibodies against CD14, CD19, CD45, CD90, and CD105 (BD Biosciences, CA, USA) and PE-conjugated antibodies against CD73 (BD Biosciences, CA, USA), were added into the centrifuge tube respectively. In this experiment, the antibodies FITC Mouse IgG1, κ Isotype Control, and PE Mouse IgG1, κ Isotype Control (BD Biosciences, CA, USA) were used as the isotype control groups for FITC-conjugated and PE-conjugated antibodies. SHEDs were incubated with antibodies in the dark for 30 min, and the results were detected using flow cytometry (BD Biosciences, CA, USA). The Flow Jo V10 software was used to analyze the expression levels of positive cells in the relevant population. The experiment was repeated at least three times using biological samples and technical means.

2.5. Osteogenic differentiation

SHEDs were collected and seeded in six-well plates. When cells achieved 80%–90% confluency, SHEDs were cultured in α-MEM containing 10% FBS, 10 mM L-glycerophosphate (Sigma-Aldrich, St. Louis, MO, USA), 100 μM dexamethasone (Sigma-Aldrich, St. Louis, MO, USA), and 50 μg/mL ascorbic acid (Sigma-Aldrich, St. Louis, MO, USA). After 21 days of culture, SHEDs were fixed with 4% polyformaldehyde for 15 min and washed with PBS. The cells were incubated with 1% alizarin red solution (Sigma-Aldrich, St. Louis, MO, USA) at room temperature for 30 min and washed with PBS. The cells were observed and photographed using a phase-contrast inverted microscope (Olympus, Tokyo, Japan). This experiment comprised at least three technical and

biological replicates.

2.6. Neurogenic differentiation

SHEDs at passage three were seeded into 24-well plates. After reaching 70% confluency, cells were cultured in a medium containing 10% FBS, 1 mM hydrocortisone (Solarbio, Beijing, China), 200 μM butylated hydroxyanisole (Sigma-Aldrich, St. Louis, MO, USA), 2 mM valproic acid (Sigma-Aldrich, St. Louis, MO, USA), 25 mM KCl (Solarbio, Beijing, China), 2 mM L-Glutamine (Sigma-Aldrich, St. Louis, MO, USA), 10 μM forskolin (Solarbio, Beijing, China), and 5 μg/mL insulin (Sigma-Aldrich, St. Louis, MO, USA), and 2% dimethyl sulfoxide (Sigma-Aldrich, St. Louis, MO, USA) for 14 days. Immunofluorescence staining was performed to detect β-III tubulin expression (1:100 dilution; Santa Cruz Biotechnology, CA, USA). Images were photographed using a fluorescence microscope (Olympus, Tokyo, Japan). The technical method and biological sample repetitions were conducted at least three times.

2.7. Cell proliferation and viability assays

A liquid extract of the TDM was collected according to the published protocol [13]. Cell proliferation assays were performed using the Cell Counting Kit-8 protocol (CCK–8C0037, Beyotime). SHEDs were prepared into a uniform cell suspension at 10^3 cells/well density and seeded in a 96-well plate. The three groups of pTDM, hTDM, and HA/TCP were set up as experimental groups with 40% and 100% leaching liquor, respectively, and the blank control group was the complete medium group. During detection, 100 μL of 10% CCK-8 reagent was added to each well and incubated at 37 °C for 2 h in the dark, and the optical density (OD) was recorded at 450 nm. Cell viability assays were performed using the CellTiter-Lumi™ II Luminescent cell viability assay kit (C0056S, Beyotime). Briefly, SHEDs were seeded in 96-well plates at a density of 10^3/well, and the leaching liquor of pTDM, hTDM, and HA/TCP was added for culturing within a specified time. The cells were lysed by adding an equal volume of CellTiter-Lumi™ II Reagent to the culture medium for 2 min at room temperature. Afterward, the supernatants were transferred into a new 96-well plate, and the luminescent signals were measured using a microplate reader (SpectraMax iD5, China).

2.8. Preparation of SHEDs/hTDM, SHEDs/pTDM, SHEDs/HA/TCP complexes

SHEDs (1×10^6) were seeded into a 3D culture system constructed using ultra-low adhesion six-well culture plates (Corning Incorporated, Corning, N·Y., USA) and hTDM scaffolds, pTDM scaffolds, and HA/TCP scaffolds [27]. The same medium as cell culture was used: α-MEM containing 10% FBS. The complexes were collected on day four for scanning electron microscopy (SEM), immunofluorescence, real-time polymerase chain reaction (RT-PCR), and animal experiments.

2.9. SEM

SEM was used to observe whether the hTDM and pTDM scaffolds completely exposed the dentinal tubules and HA/TCP scaffolds. SHEDs/hTDM, SHEDs/pTDM, and SHEDs/HA/TCP complexes were observed to understand the cell adhesion on the two TDM and HA/TCP surfaces. The scaffold samples (hTDM, pTDM, and HA/TCP) and complexes (SHEDs/hTDM, SHEDs/pTDM, and SHEDs/HA/TCP) cultured for four days *in vitro* were fixed with fixative solution (2% glutaraldehyde, Beyotime, Shanghai, China), dehydrated with ethanol, coated with gold, and observed under a scanning electron microscope (SEM, TM4000PLUS II, Hitachi, Tokyo, Japan). At least three biological samples and technical means repetitions were included. The pore areas of the exposed dentinal tubules in the SEM images of pTDM and hTDM were measured using ImageJ V1. 8.0.112 software, and the porosity was calculated as porosity = pore area/total area. At least three images were detected per sample.

2.10. Real-time PCR

The odontogenic differentiation-related gene expression was detected using Real-time PCR. SHEDs served as the blank control group, SHEDs/HA/TCP served as the negative control group, and SHEDs/hTDM and SHEDs/pTDM served as the experimental groups. RNAiso Plus (Takara Biomedical Technology, Beijing, China), PrimeScript™ RT reagent (Takara Biomedical Technology, Beijing, China), and SYBR Premix (QIAGEN, Hilden, Germany) were used to extract total RNA, reverse transcribe RNA to cDNA, and detect the related genes' expression levels (*DSPP*, *POSTN*, *TGF-β1*, *ALP*, *COL-1*, *OCN*, and *RUNX2*). According to the instructions, the configuration of each 10 μL PCR reaction solution contained 5 μL SYBR Premix, 0.4 μL PCR forward primer, 0.4 μL PCR reverse primer, 1 μL DNA template, and 3.2 μL sterile water. After normalization to the GAPDH internal reference gene, relative mRNA expression was determined using the $2^{-\Delta\Delta CT}$ method. Supplemental Table 1 displays Real-time PCR primer sequences. The experiment was repeated at least three times using biological samples and technical means.

2.11. Immunofluorescence staining

The odontogenic differentiation-related proteins' expression levels were detected using immunofluorescence. SHEDs/hTDM, SHEDs/pTDM, and SHEDs/HA/TCP were cultured *in vitro* for four days, washed 2–3 times with PBS, fixed with paraformaldehyde for 10 min, treated with 0.1% Triton for 5 min and blocked with 1% BSA for 30 min. Primary antibodies, including DSPP, DMP1, CAP, TGF-β1, and PBS, were incubated with samples overnight in a humidified chamber at 4 °C. The samples were washed with PBS three times, incubated with Alexa Fluor® 488 goat anti-mouse antibody for 1 h, stained with DAPI for 5 min, observed under a confocal microscope (Leica Optical, Wetzlar, Germany), and photographed. ImageJ V1. 8.0.112 software was used to semi-quantitatively analyze specific protein expressions and detect the average fluorescence intensity of at least three fluorescence images in the same group under different visual fields. The experiment was repeated at least three times using biological samples and technical means.

2.12. Subcutaneous implantation

SHEDs/hTDM and SHEDs/pTDM complexes were implanted into the left and right sides of longitudinal incisions on the back of nude mice (eight-week-old male, n = 6) under isoflurane anesthesia to verify further the odontogenic differentiation ability of the two complexes *in vivo*. SHEDs/HA/TCP served as the control scaffold, and histological staining was performed to evaluate hTDM and pTDM before subcutaneous implantation. The numbers of implants were as follows: SHEDs/hTDM (n = 6), SHEDs/pTDM (n = 6), and SHEDs/HA/TCP (n = 6). After eight weeks, subcutaneous graft samples were collected, decalcified with 10% EDTA for seven to eight months, dehydrated, embedded, and paraffin-sectioned. Hematoxylin-eosin (H&E, Solarbio, Beijing, China) and Masson's Trichrome staining (Solarbio, Beijing, China) were used to observe the morphological changes. The formation of a pulp-dentinal complex in subcutaneous transplantation samples was evaluated using immunofluorescence staining. The primary antibodies used were DSPP, DMP1, CAP, TGF-β1, and β-III tubulin. ImageJ V1. 8.0.112 software was used to semi-quantitatively analyze specific protein expressionexpressions and detect the average fluorescence intensity of at least three fluorescence images in the same group under different visual fields.

2.13. Proteomics

Two samples of pooled porcine TDM were used for quantitative proteomic analysis. The experimental methods of sample processing, sodium dodecyl sulfate-polyacrylamide gel electrophoresis (SDS-PAGE), filter-aided sample preparation (FASP) enzymatic hydrolysis, and liquid chromatography-mass spectrometry (LC-MS) in the proteomic analysis followed those in our published article [28].

2.13.1. Sample processing and SDS-PAGE

An appropriate amount of the SDT lysis solution was added to the samples. The samples were sonicated and bathed in boiling water for 10 min. The samples were centrifuged, and the supernatants were collected.

2.13.2. FASP enzymatic hydrolysis

DTT was added to 200 μg of the protein solution to obtain a final concentration of 100 mM. Then, the solution was boiled in water for 5 min and cooled to room temperature. After discarding the filtrate, 100 μL of IAA buffer (100 mM IAA in UA), 100 μL of UA buffer, 100 μL of 25 mM NH_4HCO_3, and 40 μL trypsin buffer solution was centrifuged at 14,000×*g* for 15 min after each addition of buffer. Briefly, 40 μL of 25 mM NH_4HCO_3 was centrifuged at 14,000×*g* for 15 min, and the filtrate was collected. The peptides were desalted using a C18 Cartridge, lyophilized, and quantified (OD280).

2.13.3. LC-MS mass spectrometry

According to the quantitative results, an appropriate amount of enzymatic hydrolysis product was used for LC-MS/MS analysis, and each sample was injected once. The samples were loaded onto a chromatographic column (Thermo Fisher Scientific, Waltham, MA, USA) and separated using an analytical column (Thermo Fisher Scientific, Waltham, MA, USA). The peptides were separated using chromatography and analyzed using mass spectrometry and a Q-Exactive mass spectrometer (Thermo Fisher Scientific, Waltham, MA, USA).

2.13.4. Mass spectrometry data analysis

The raw files were database retrieved using MaxQuant software. The protein databases were uniprot_Sus_scrofa_122045_20210125 (total number of sequences: 122045, download time: 20210125, download link: http://www.uniprot.org) and uniprot_sus_scrofa_122027_20200901 (total number of sequences: 122027, download time: 20200901, download link: http://www.uniprot.org). The database search parameters were set as follows: trypsin was the enzyme, missed cleavage sites were set to two, the fixed modification was carbamidomethyl (C), and dynamic modification was set to oxidation (M) and acetyl (Protein N-term). The proteins identified by the database search must meet the set filter parameter FDR ≤0.01.

2.13.5. Bioinformatics analysis

Functional protein analysis was performed using the DAVID database (https://david.ncifcrf.gov) and the Kyoto Encyclopedia of Genes and Genomes (KEGG). Protein-protein interaction (PPI) networks were generated using STRING (https://string-db.org) for hTDM, pTDM, and coexisting protein lists. The PPI networks of hTDM and pTDM were visualized using Cytoscape. The hTDM network was divided into six clusters using the k-means algorithm. The pTDM and the coexisting networks were divided into three clusters using k-means algorithm. Proteins unconnected in the networks were ignored in the network illustrations. For each cluster in the three networks, Gene ontology (GO) biological process enrichment analyses were performed using BiNGo [29]. Bonferroni (FWER) correction was adopted for multiple testing corrections, and adjusted P-values were used to measure enrichment.

Phylogenetic analyses were performed on the obtained protein sequences from the hTDM (blue) and pTDM (red) protein lists. MUSCLE [30] was adopted for multiple sequence alignment. The phylogenetic tree was visualized using iTOL [31]. Correlations were calculated based on corresponding branch distances in the phylogenetic tree. The sequence similarity analysis was performed using protr R package to further evaluate the homology in amino acid sequences between hTDM and pTDM [32]. The pairwise similarity values were calculated based on the Smith-Waterman local sequence alignment. In the similarity analysis of the obtained protein sequences of pTDM, pairwise similarity values for each obtained protein sequence (n = 392) of hTDM were calculated for each pTDM protein sequence (n = 67). Then, the most matched human gene was selected, and the similarity value of the gene pair was obtained. Finally, 67 similarity values were collected and displayed.

CHAT [33] analyses were performed to further explore the differences in the detected protein quantity distribution between the coexisting protein lists for hTDM and pTDM. First, *in silico* digestion (trypsin digestion, mis-cleavage number 2) was performed on the obtained protein sequences using the rpg [34] python package to quantify the proteins for CHAT. Second, the protein iBAQ values were calculated by dividing the sum of the peptide intensities by the number of theoretically observable peptides with lengths between 6 and 30 amino acids. For CHAT analysis, the calculated protein expressions were treated as the contextual information of the proteins. The top 36 abundant proteins were treated as contexture important genes. Important contextual hub genes (in circles) for each protein list were subsequently inferred, indicating significant pathways potentially affected by the protein distributions of the two TDM samples.

2.14. Statistical analysis

The data were displayed as mean ± standard deviation (SD). Statistical differences were assessed using one-way analysis of variance (ANOVA) or Student's t-test. All statistical graphs were analyzed and produced using GraphPad Prism software. P-values <0.05 were considered statistically significant.

3. Results

3.1. Comparison of the structure of hTDM, pTDM, and HA/TCP

The SEM results demonstrated that hTDM and pTDM effectively exposed the dentinal tubules after gradient concentration EDTA treatment and HA/TCP surface (Fig. 1A a, b, and e). Furthermore, SEM analysis of the SHEDs/hTDM and SHEDs/pTDM complexes confirmed that the cells exhibited uniform and dense growth on both scaffolds (Fig. 1A c and d). Conversely, only a small number of cells adhered to the SHEDs/HA/TCP complex surface (Fig. 1A f). According to phalloidin immunofluorescence staining, the cells showed uniform and dense adhesion on the surface of pTDM and hTDM but only a small amount of adhesion on the HA/TCP material in the control group (Fig. 1B). The cell proliferation and viability assays confirmed that TDM has a certain promoting effect on the growth of SHEDs in the early stage. It may be due to the fact that the protein components released by TDM have a certain promoting effect on the growth of cells, but this promoting effect will decrease with the increase of observation time (Fig. 1G and H). The functional groups of pTDM and hTDM were determined using FTIR. The peak near 3440 cm^{-1} indicated the presence of hydroxyapatite, and the peak in the range of 1441–1635 cm^{-1} indicated the presence of carbonate (Fig. 1C). The organic and inorganic components of the pTDM and hTDM were measured using a Raman spectrometer. The peaks at 422, 585, and 962 cm^{-1} correspond to $PO4^{-3}$, a dentin mineral. The peaks in the ranges 1220–1300, 1455~1320, and 1550~1720 cm^{-1} belong to amide III, CH, and amide I, respectively (Fig. 1D). FTIR and Raman results present that pTDM and hTDM have a high similarity in chemical structure.

3.2. SHEDs culture and characterization

Flow cytometry results revealed specific marker expression of

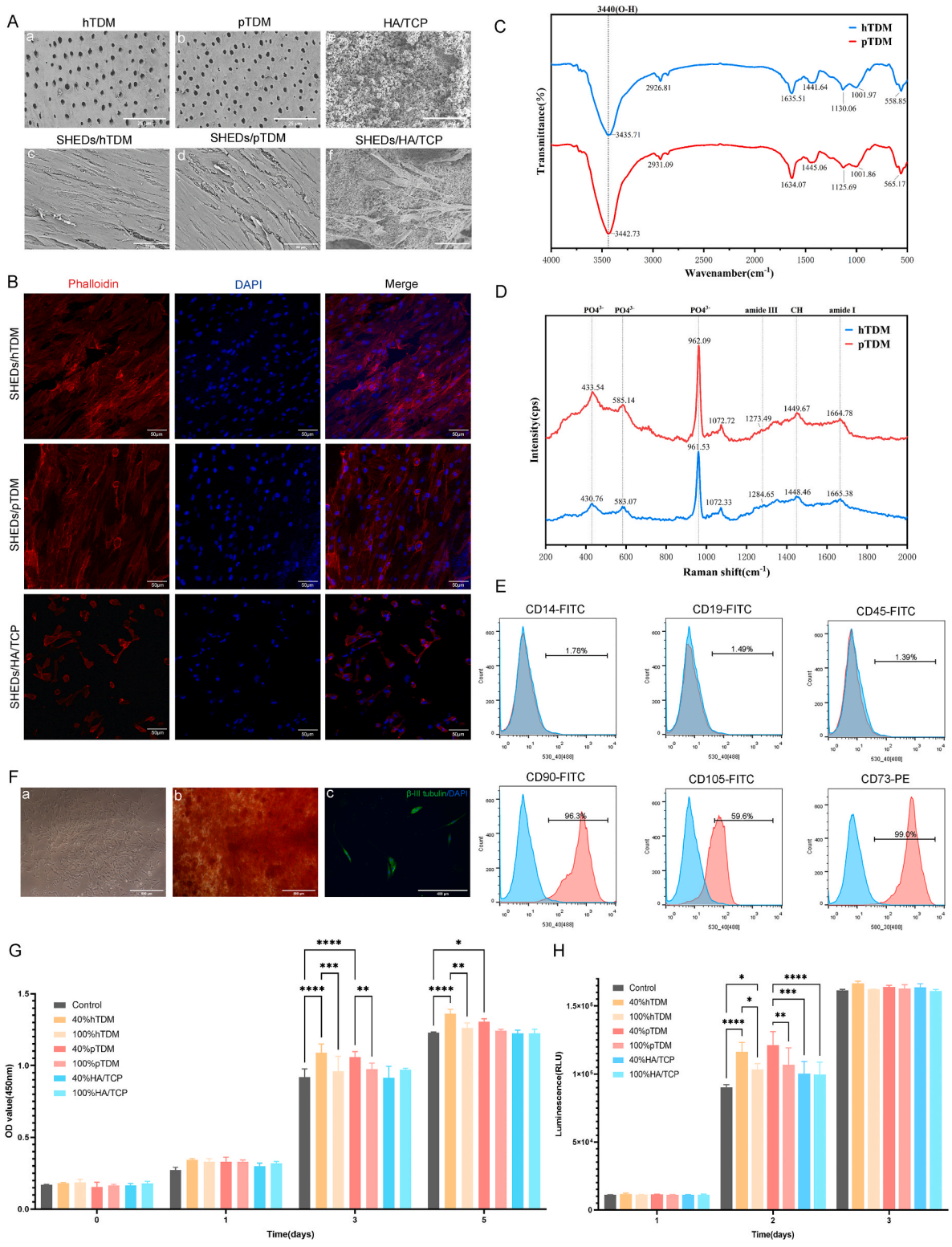

Fig. 1. Structure characterization analysis of pTDM and hTDM and characterization of SHEDs. (A, a and b) hTDM and pTDM dentinal tubules were completely exposed. (A c, and d) The adhesion of SHEDs on hTDM and pTDM surfaces was detected by SEM. (A e) The porosity of hTDM and pTDM were higher than that of HA/TCP. (A f) The adhesion of SHEDs on hTDM and pTDM were more than that of HA/TCP. Scale bars = 25 μm (A, a, b and e), scale bars = 50 μm (A c, d and f). (B) Immunofluorescence staining of SHEDs/hTDM, SHEDs/pTDM, SHEDs/HA/TCP complexes. Scale bars = 50 μm. (C) The functional groups of hTDM and pTDM were determined by the FTIR. (D) Organic and inorganic components of hTDM and pTDM were measured by Raman spectroscopy. (E) The expression of immunophenotype markers in SHEDs. (F a) The morphology of primary SHEDs. (F b) Alizarin red staining was used to detect the osteogenic differentiation of SHEDs. (F c) The expression of β-III tubulin was used to detect the neurogenic differentiation of SHEDs. Scale bars = 500 μm (F a and b), scale bar = 400 μm (F c). (G) Cell proliferation was assessed daily for 5 days with the CCK-8 assay. (H) Viability of SHEDs were measured by the CellTiter-Lumi™ II Luminescent cell viability assay. *$p < 0.05$, **$p < 0.01$, ***$p < 0.001$, ****$p < 0.0001$. (For interpretation of the references to colour in this figure legend, the reader is referred to the Web version of this article.)

mesenchymal stem cells in SHEDs as follows: CD90 (96.3%), CD105 (59.6%), and CD73 (99.0%). Additionally, the monocyte marker CD14 was expressed at 1.78%, while the B-cell marker and leukocyte marker CD45 were expressed at 1.49% and 1.39%, respectively (Fig. 1E). The primary SHEDs exhibited a fibroblast-like spindle shape (Fig. 1F a). The multilineage differentiation potential of SHEDs was also assessed. The osteogenic differentiation ability of SHEDs was evaluated using alizarin red staining, demonstrating the numerous calcium nodule formation following osteogenic induction (Fig. 1F b). When cultured in neuroblast-inducing conditions, SHEDs differentiated into nerve-like cells and exhibited positive expression of the neuronal marker, β-III tubulin (Fig. 1F c).

3.3. Effects of two scaffolds on odontogenic differentiation of SHEDs in vitro

RT-PCR results revealed changes in relevant mRNA levels. After four days of co-culture with the two types of TDM, *DSPP* expression was approximately three-fold higher in the SHEDs/hTDM complex than in the SHEDs and SHEDs/HA/TCP groups. Similarly, *DSPP* expression was 1.5-fold higher in the SHEDs/pTDM complex than in SHEDs (Fig. 2A). *POSTN* mRNA expression level was significantly elevated in the SHEDs/hTDM complex than in SHEDs and SHEDs/HA/TCP complexes, but there was no significant difference between the SHEDs/hTDM and SHEDs/pTDM complexes (Fig. 2A). *TGF-β1* expression increased approximately 10-fold in SHEDs/hTDM and SHEDs/pTDM complexes than in SHEDs and SHEDs/HA/TCP complexes. However, *ALP* expression was 0.1-fold higher in the SHEDs/hTDM and SHEDs/pTDM complexes than in the SHEDs and SHEDs/HA/TCP complexes (Fig. 2A). *COL-1* expression was approximately 1.5-fold higher in SHEDs/pTDM complex than in SHEDs and SHEDs/HA/TCP complex, with no significant difference observed between SHEDs/hTDM and SHEDs/pTDM complexes (Fig. 2A). Furthermore, *OCN* mRNA expression increased approximately eight-, six- and four-fold in SHEDs/pTDM, SHEDs/hTDM, and SHEDs/HA/TCP complexes than in SHEDs, respectively (Fig. 2A). Additionally, *RUNX2* expression increased approximately three-fold in SHEDs/hTDM and SHEDs/pTDM complexes than in SHEDs and SHEDs/HA/TCP complexes (Fig. 2A).

Immunofluorescence staining and quantitative analysis revealed that the SHEDs/hTDM and SHEDs/pTDM complexes exhibited odontogenic marker expression, including DSPP, DMP1, CAP, and TGF-β1, after culturing for four days *in v*itro. However, these markers were not expressed in SHEDs/HA/TCP complexes (Fig. 2B a). The DSPP and DMP1 expression did not differ significantly between SHEDs/hTDM and SHEDs/pTDM (Fig. 2B b). CAP and TGF-β1 expression levels were approximately one-fold higher in SHEDs/hTDM than in SHEDs/pTDM (Fig. 2B b). We observed no positive staining in the PBS control group (Supplemental Fig. 1).

3.4. SHEDs combined with hTDM or pTDM induced regeneration of dentin-pulp tissue

H&E and Masson's Trichrome staining displayed that the cementum, dentin-pulp tissues, and pre-dentin have been removed in hTDM and pTDM before transplantation (Supplemental Fig. 2). Following the eight-week subcutaneous transplantation of the SHEDs/hTDM and SHEDs/pTDM complexes into nude mice, samples were collected. H&E and Masson's trichrome staining (Fig. 3C) revealed the presence of pulp-like tissue within the lumens of both TDM types, indicated by a blue square. Additionally, new blood vessel formation was observed in pulp-like tissue. Notably, dentin-like structures were consistently formed on the inner and outer surfaces of the TDM scaffolds, as denoted by yellow arrows (Fig. 3C). The yellow dotted lines marked the demarcation between the newly formed dentin-like tissue and the TDM structure (Fig. 3C). Fibrous structures were observed on the exterior of the complexes. Fiber-like tissue was observed in the HA/TCP scaffold group, but a root-related structure was not formed (Fig. 3C). The results of immunofluorescence staining and semi-quantitative analysis showed that SHEDs/hTDM and SHEDs/pTDM complexes were similar in the expression of DMP1, CAPTGF-β1, and β-III tubulin neurogenic markers. (Fig. 3A and B).

3.5. Proteomic analysis

3.5.1. Protein composition of pTDM

Supplemental Table 2 indicates that 189 protein groups are detected in shotgun1 proteomic, while 109 protein groups are detected in shotgun2 proteomic analysis. According to the proteomic result, 20 protein groups were identified in both shotgun proteomics analyses, and 278 protein groups were detected in pTDM. A total of 15 types of collagens were identified and ranked based on their content: COL1A1, COL1A2, COL18A1, COL5A2, COL5A1, COL4A4, COL11A1, COL22A1, COL11A2, COL7A1, COL12A1, COL6A2, COL15A1, COL6A3, and COL21A1. Additionally, seven kinds of CD molecules were included in the analysis: CD44, CD200, CD276, CD59, CD63, CD58, and CD47. The top 10 enriched GO terms in biological processes, cell composition, and molecular functions were cell adhesion, ECM organization, extracellular space, extracellular region, ECM structural constituent, and heparin binding (Fig. 4A). KEGG analysis revealed that the top 10 significantly enriched pathways included ECM-receptor interaction, complement and coagulation cascades, protein digestion and absorption, and focal adhesion (Fig. 4B).

3.5.2. Comparison of the protein composition of pTDM and hTDM

The hTDM sample contained 708 protein groups, 12 of which were collagen proteins. Among these collagen proteins, COL1A1 and COL1A2 had the highest content [28]. Only 278 proteins were identified in the pTDM sample, but the top two collagen proteins with the highest content were COL1A1 and COL1A2, consistent with hTDM findings. Furthermore, when comparing the proteome analysis of hTDM [28], 58 coexisting proteins were found in both TDM scaffolds (Fig. 4C). These coexisting proteins included COL1A1, COL5A2, COL6A3, COL5A1, COL6A2, POSTN, F2, and AHSG (Supplemental Table 2), which are among the top 10 core proteins in the pTDM protein interaction network. Among the 58 coexisting proteins, COL1A1, COL1A2, POSTN, and DSPP were most closely associated with odontogenic differentiation proteins. According to the iBAQ results of the top 20 hTDM proteomes, Alpha-2-HS-glycoprotein had the highest content in hTDM proteomes, ranking eighteenth in pTDM proteomes. Additionally, serum albumin and vitronectin had high iBAQ values (Fig. 4D). According to the iBAQ results of the top 20 pTDM proteomes, collagen alpha-1 (I) chain pre-proprotein and fibrillar collagen NC1 domain-containing protein ranked first and second, respectively. Besides, phosphate transporter, CD44 antigen, and histone acetyltransferase had high iBAQ values (Fig. 4E). GO analysis revealed that the 58 coexisting proteins were primarily enriched in the extracellular space, extracellular region, ECM structural constituents, and collagen fibril organization (Fig. 4F). Additionally, KEGG analysis demonstrated that these proteins were predominantly enriched in pathways such as ECM-receptor interaction, protein digestion and absorption, complement and coagulation cascades, focal adhesion, proteoglycans in cancer, and the PI3K-Akt signaling pathway (Fig. 4G).

3.5.3. Interaction network analyses of TDM proteomes

Proteins in hTDM (Fig. 5A) and pTDM (Fig. 5B) engaged in direct interactions, forming a highly interconnected network. Among the collagen proteins, COL1A1 and COL1A2 have a high number of nodes in the PPI of hTDM and pTDM. Furthermore, CD44 and LUM had a high number of nodes in hTDM, and ALB, BGN, and LUM had a high number of nodes in pTDM. This suggests that these highly connected proteins may be key to the metabolic and signal transduction pathways. Network clustering analysis in hTDM revealed six subnetworks enriched in ECM

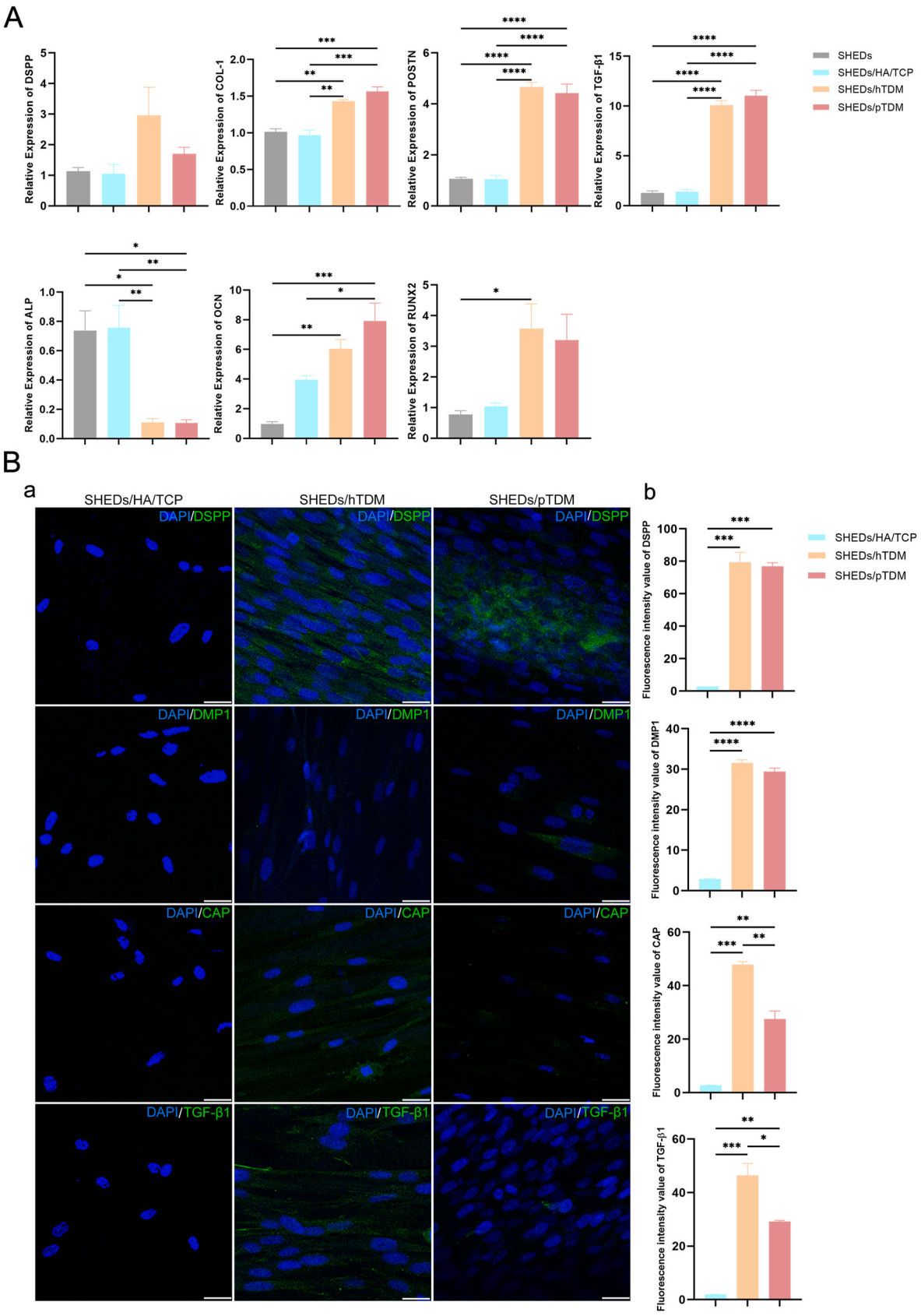

Fig. 2. Expression levels of odontogenic related markers in SHEDs/hTDM , SHEDs/pTDM and SHEDs/HA/TCP complexes. (A) Expression levels of *DSPP*, *DMP1*, *POSTN*, *TGF-β1*, *ALP*, *COL-1*, *OCN*, and *RUNX2* in SHEDs/TDM complexes. (B a) Expression levels of DSPP, DMP1, CAP, and TGF-β1 in SHEDs/TDM and SHEDs/HA/TCP complexes were detected by immunofluorescence. (B b) Quantification of DSPP, DMP1, CAP, and TGF-β1 protein expression. Scale bars = 25 μm *p < 0.05, **p < 0.01, ***p < 0.001, ****p < 0.0001.

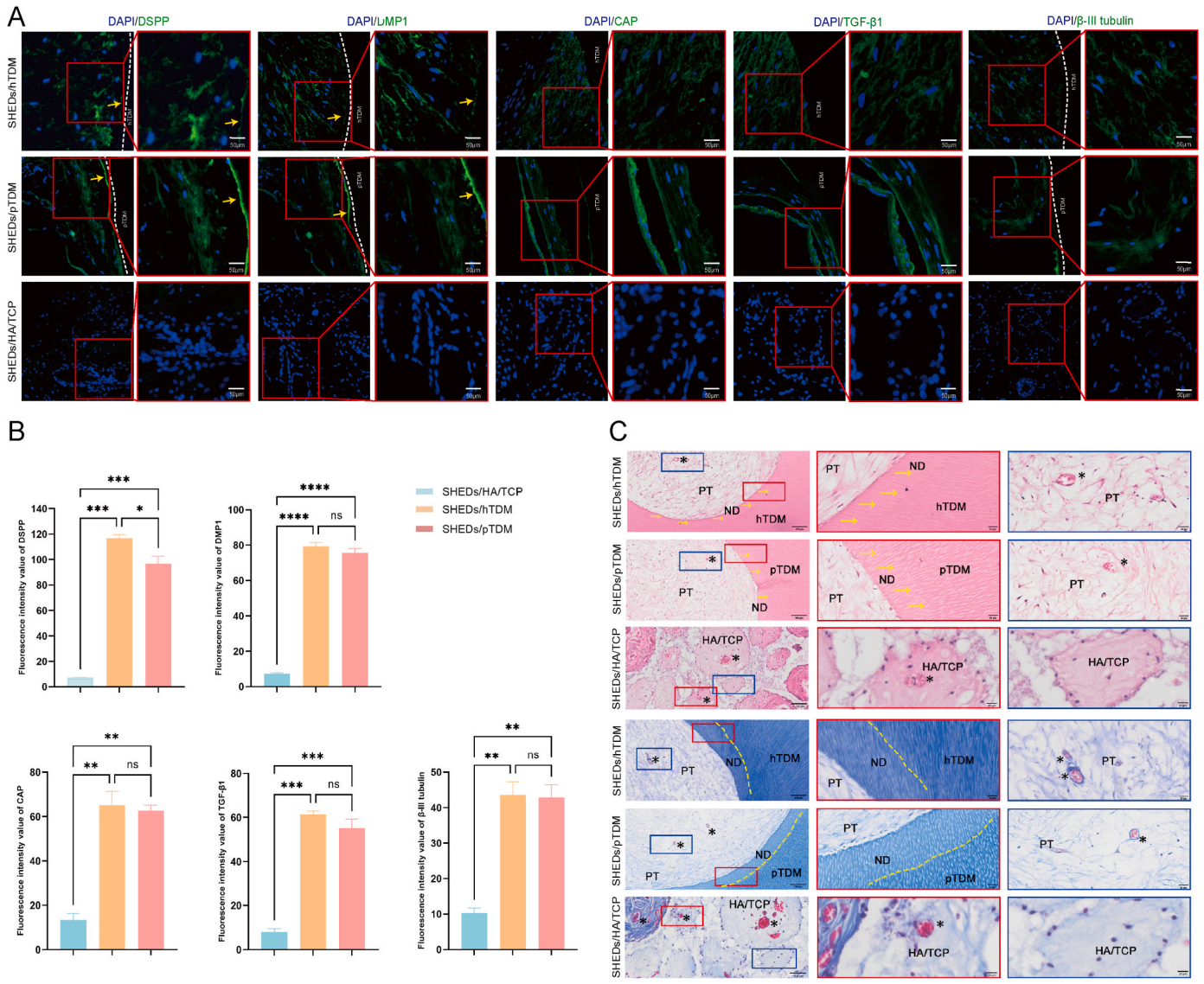

Fig. 3. Immunofluorescence, H&E, and Masson's Trichrome staining of samples 8 weeks after subcutaneous transplantation in nude mice. (A) Immunofluorescence staining showed that there were dentin-specific proteins and neurogenic proteins in SHEDs/TDM complexes. Scale bars = 50 μm. (B) Quantification of DSPP, DMP1, CAP, TGF-β1 and β-III tubulin protein expression. *p < 0.05, **p < 0.01, ***p < 0.001, ****p < 0.0001. (C) H&E staining and Masson's Trichrome staining showed that root-associated regenerative tissues were observed in SHEDs/TDM complexes. PT: pulp tissue, ND: new dentin, hTDM: human treated dentin matrix, pTDM: porcine treated dentin matrix, FL: fiber-like tissues, *: blood vessel, yellow arrows, and yellow dotted line indicated the newly formed dentin like tissue area. The first and fourth columns (scale bars = 100 μm), and the second, third, fifth and sixth columns (scale bars = 20 μm). (For interpretation of the references to colour in this figure legend, the reader is referred to the Web version of this article.)

organization, actin filament organization, translation, RNA splicing, regulation of cholesterol esterification, and humoral immune response (Fig. 5D). Network clustering analysis in pTDM revealed three subnetworks enriched in biomineral formation, collagen fibril organization, and acute inflammatory response (Fig. 5E). The proteins that coexisted in both TDMs were enriched in the three subnetworks (Fig. 5F). Supplemental Table 3 lists the top 10 hub genes for each protein network. The phylogenetic tree revealed the presence of numerous evolutionarily conserved proteins between the two species, including ACTG1, PHEX, LUM, and COL6A3 (Fig. 5C and Supplemental Table 4). Sequence similarity analysis indicated that most of the porcine genes in pTDM exhibited low sequence similarities to all the obtained protein sequences in hTDM. When matched to a human protein sequence from hTDM, only 12% of the pTDM genes displayed a similarity value over 0.85, while only 15% of the pTDM genes exhibited a similarity value over 0.70. (Supplemental Fig. 3). The CHAT analyses showed significant variations in the important contextual hub genes obtained from the network, which can be attributed to inconsistencies in protein abundance (Fig. 5G–H). The shared contextual hubs, PITX3 and MMP20, were identified for both hTDM and pTDM.

4. Discussion

ECM-based bioscaffolds have shown promise as scaffold materials. Previous studies have utilized hTDM as a scaffold material for bio-root construction. However, the acquisition of a substantial quantity of hTDM poses challenges. pTDM is a good substitute for hTDM due to the similar differentiation induction. Therefore, it would be advantageous to identify specific protein components of pTDM. This knowledge will facilitate the utilization of pTDM in bio-root construction and guide the synthesis of artificial ECM scaffolds.

The results of this study demonstrate that pTDM and hTDM have higher porosity, which is crucial in facilitating adherent cell adhesion, nutrient transportation, and cell growth promotion [35,36]. The porous

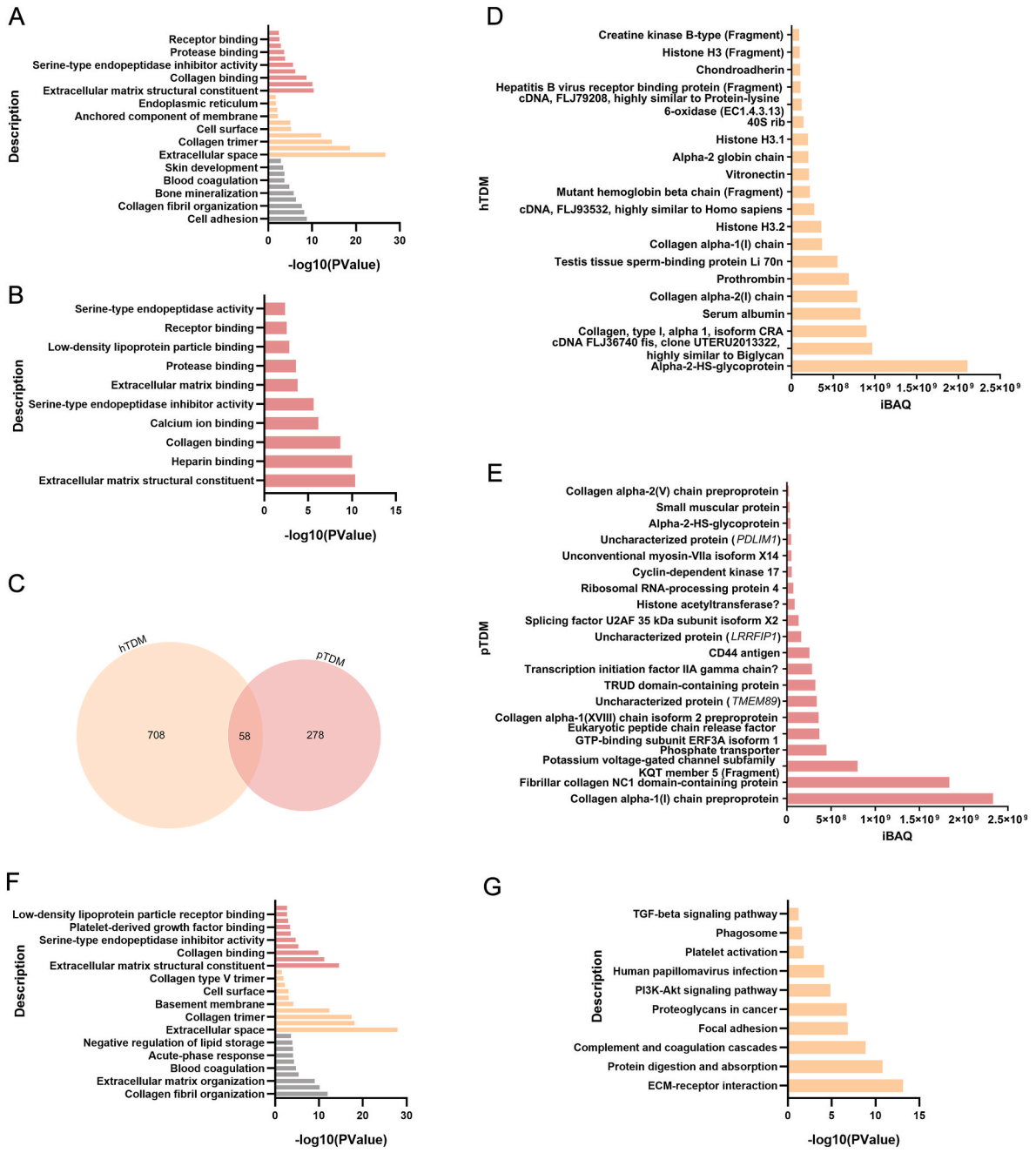

Fig. 4. GO, KEGG and iBAQ value analysis of TDM proteomes. (A) Gene Ontology (GO) enrichment of pTDM proteome. (B) Kyoto Encyclopedia of Genes and Genomes (KEGG) enrichment of pTDM proteome. (C) Venn diagram of hTDM and pTDM proteomes. (D) Analysis of iBAQ value of hTDM. (E) Analysis of iBAQ value of pTDM. (F) GO enrichment of the 58 proteins coexisting in pTDM and hTDM. (G) KEGG enrichment of the 58 proteins coexisting in pTDM and hTDM.

structure is of utmost importance for TDM, as it effectively releases odontogenic growth factors and proteins, thereby promoting close adhesion to cells, exhibiting favorable biocompatibility, and facilitating cell growth and proliferation. Immunofluorescence staining of phalloidin, and cell proliferation and viability experiments confirmed that SHEDs had excellent adhesion ability in TDM, and TDM also promoted SHED growth. The FTIR and Raman results showed that pTDM and hTDM have highly similar chemical structures. pTDM and hTDM have great similarities in their physical morphology and chemical structure, suggesting that pTDM has potential as an alternative to hTDM.

ALP, *COL-1*, and *RUNX2* are osteogenesis and mineralization markers closely associated with calcium phosphate mineral formation in cementum and dentin [37,38]. *TGF-β1* is a marker of periodontal ligament tissue maintenance and regeneration [39]. The protein derived mainly from DSPP dominates the non-collagenous protein in dentin [40]. DSPP and DMP1 are specific markers in dentin and play crucial roles in dentin formation [41,42]. This study's findings displayed a similar upregulated expression trend of odontogenic differentiation-related mRNAs in SHEDs induced by both TDM scaffolds but not in HA/TCP group. Regarding odontogenesis-related proteins, DSPP and DMP1 expression levels were consistently observed in SHEDs induced by both scaffolds. This finding indicates that pTDM can stimulate odontogenic differentiation of SHEDs *in vitro* and exerts a similar induction effect as hTDM. Furthermore, the outcomes of the animal experiment suggest that pTDM, like hTDM, has a comparable impact on the regeneration of root-related tissues with an odontogenic effect. These findings imply that pTDM creates a microenvironment conducive to odontogenesis, facilitating bio-root regeneration.

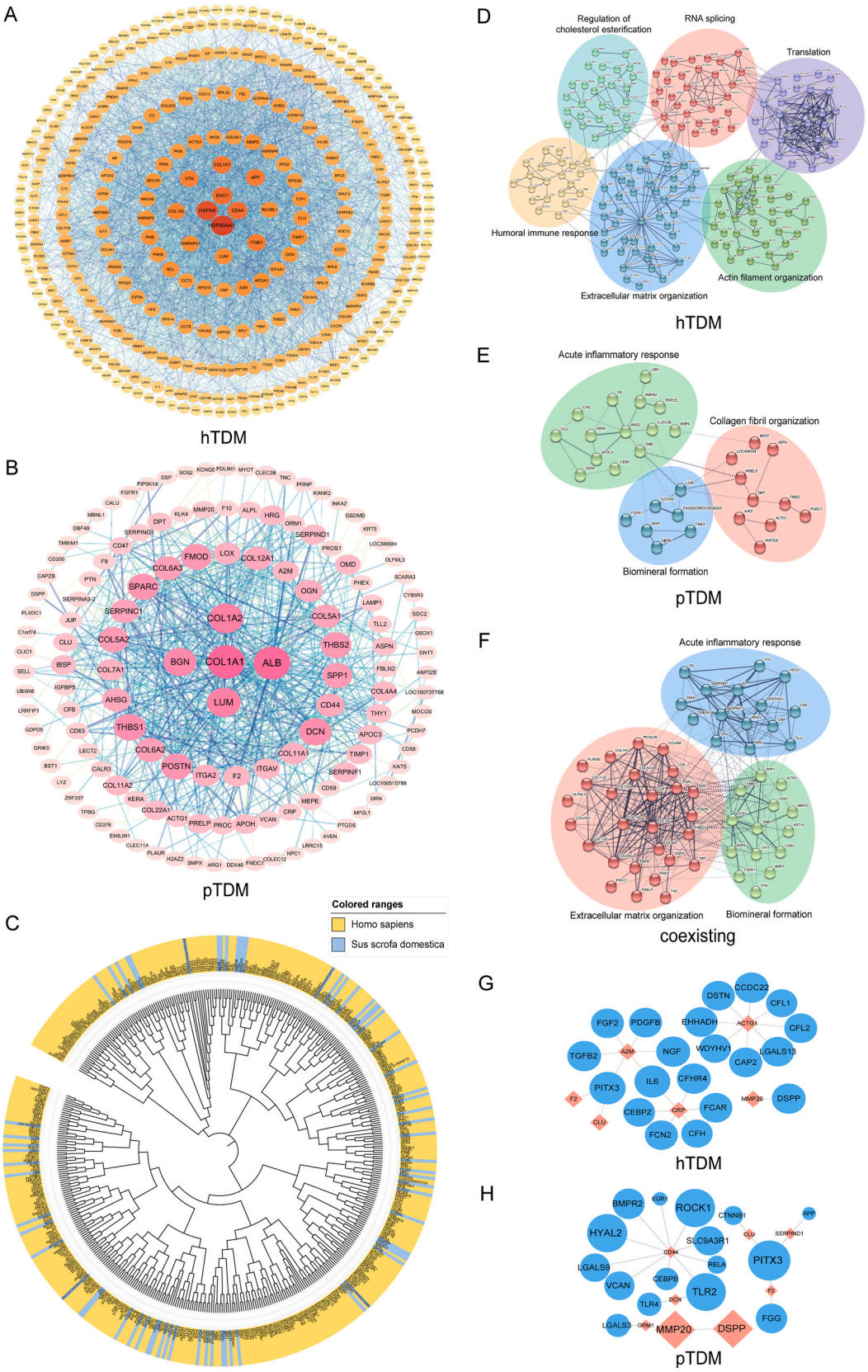

Fig. 5. Interaction network analyses of TDM proteomes. The Protein-Protein Interaction networks of hTDM (A) and pTDM (B) protein lists. (C) Phylogenetic tree of the obtained protein sequences of the hTDM (yellow) and pTDM (blue) protein list. The network clustering analysis of hTDM (D), pTDM (E) and the coexisting (F) protein lists. CHAT analyses of the coexisting proteins of hTDM (G) and pTDM (H), the size of nodes represents the significance of the genes. (For interpretation of the references to colour in this figure legend, the reader is referred to the Web version of this article.)

Bioinformatic analysis was conducted on the proteome of pTDM and previously obtained hTDM proteome datasets to explore the mechanisms by which TDM components regulate tooth root regeneration [28]. Proteomic analysis of pTDM revealed 278 groups of proteins, indicating a lower count than hTDM. This disparity can be attributed to comparing protein expressions between different species. Additionally, the reliability and accuracy of protein sequence-related databases are crucial factors to consider for less-extensively studied species [43,44]. Notably, collagen is the most abundant protein in both TDMs, with COL1A1 and COL1A2 exhibiting the highest levels. COL1A1 serves as a marker of bone mineralization [45]. COL1A2 is an early indicator of osteogenesis and an important marker of bone healing [46–49]. The presence of these collagens greatly influences the calcium and phosphorus composition within the hard tissue formed by cells adhered to the surface of TDM during the bio-root regeneration. Besides that, we find that Alpha-2-HS-glycoprotein had the highest content in hTDM proteomes and ranked high in pTDM proteomes. Alpha-2-HS-glycoprotein, also known as fetuin-A, is the main glycoprotein in the bones and teeth [50]. Fetuin-A can affect calcification by inhibiting mineralization [49,51–53] and may play a role in the mineralization of peritubular dentin [54]. Although there are many coexisting proteins in pTDM and hTDM, sequence similarity analysis shows that the two protein sequences have low sequence similarity. Therefore, functional differences caused by the similarity of the two protein sequences must also be considered.

ECM molecules are categorized as collagen, elastin, proteoglycans, or other non-collagen glycoproteins. The results of the bioinformatics analysis demonstrated that some proteins were present in pTDM but not in hTDM, suggesting some structural and functional differences. For example, pTDM contains collagen type XXI alpha 1, collagen alpha-1 (XV) chain isoform X1, collagen alpha-1 (XVIII) chain isoform 2 preproprotein, collagen alpha-2 (XI) chain isoform X1, and collagen IV NC1 domain-containing protein. Collagen XXI is present in tissues containing abundant ECM and maintains the ECM integrity [55]. Type XV collagen has a wide tissue distribution and is significantly expressed in osteoblasts [56]. CD44, fibronectin, bone sialoprotein 2 (BSP2), matrix extracellular phosphoglycoprotein (MEPE), and alkaline phosphatase (ALP) are the glycoproteins of pTDM. CD44 is involved in the early mineralization of odontoblasts and may play a key role in the initial mineralization of tooth-related structures [57]. Fibronectin is crucial in odontoblast differentiation during tooth development [58]. BSP2 is a key regulator of mineralized tissue formation found almost exclusively in mineralized connective tissues [59,60], and it may play a role in enamel formation and subsequent mineralization [61]. MEPE has a potential regulatory effect on tooth matrix formation and mineralization [62]. ALP is the most widely recognized marker of osteoblast activity. pTDM also contains other proteins related to osteogenesis and odontogenesis, such as phosphate transporters, histone acetylation, insulin-like growth factor binding protein-5 (IGFBP-5), and Dickkopf WNT signaling pathway inhibitor 3 (Dkk3). Phosphate is an essential component of hydroxyapatite crystals. Phosphate transporters are involved in the late stages of tooth development and mineralization [63]. Histone acetylation plays a crucial role in the odontogenic differentiation of mesenchymal stem cells [64]. IGFBP-5 can enhance the neurogenic and odontogenic differentiation of dental stem cells [65]. Wnt signaling is essential for odontogenesis. Dkk3 can play a role in tooth formation by regulating the Wnt signaling pathway [66]. We speculate that these differences may be partly due to the proteins in the pTDM. Therefore, these proteins are essential clues to explore the difference between pTDM and hTDM, but their verification needs more research in the future.

The most significantly enriched terms associated with ECM did not surpass our initial expectations, consistent with TDM being an ECM-based biomaterial. Additionally, odontogenesis-related proteins were present in the coexisting proteins. For example, DSPP is a specific marker in dentin [42] that interacts with MMP20 (Fig. 5E and F), indicating that the DSPP-MMP20 interaction is vital for new dentin formation [67]. POSTN, one of the top 10 hub genes, is associated with the functionality of the periodontal ligament [68]. Moreover, evolutionarily conserved proteins were identified, indicating similar biological functions. For example, mutated or absent PHEX leads to severe hypomineralization of both bones and teeth [69]. Fibromodulin (FMOD) and lumican (LUM) are small leucine-rich proteoglycans (SLRPs) that serve as key regulators in controlling periodontal development and homeostasis [70]. FGFR1 signaling has been revealed as a new mechanism during the odontogenic differentiation of human dental stem cells [71,72]. The amino acid sequence homology analysis suggested that these proteins might be responsible for providing a similar organic odontogenesis microenvironment. CHAT analysis showed that important contextual hub genes obtained from the network varied significantly due to the protein abundance inconsistency, indicating the potential differences in the underlying mechanisms between the two species and highlighting the possibility of enhancing the application value of pTDM by adjusting the protein composition formula. Notably, the common contextual hub PITX3 for hTDM and pTDM warrants further investigation because the PITX family has been linked to tooth development [73]. Therefore, these hub proteins or networks are key to the odontogenesis microenvironment; however, their validation requires further research.

Furthermore, pTDM proteomes contain numerous proteins involved in the immune response. Hyaluronic acid, an essential polysaccharide component of vertebrate ECM, is recognized by CD44 as a receptor. One potential approach to reduce inflammation is to increase the clearance of hyaluronic acid [74]. The complement regulatory protein CD59 [75], also known as a reactive membrane attack complex inhibitor, prevents the formation of membrane attack units and inhibits the terminal complement attack response. CD58 is an immune adhesion molecule, and cell adhesion is critical for immune responses [76]. It is plausible that these immune-related CD molecules identified in the proteome could potentially catalyze the inflammatory response triggered by the xenogeneic TDM (pTDM) mentioned in the preceding study in conjunction with the *in vivo* transplantation of allogeneic DFCs [22]. Additionally, a cluster of coexisting proteins exhibited notable enrichment in the acute inflammatory response, suggesting their potential to induce an immune response. One viable approach to circumvent immune rejection involves implementing a gene-knockout technique [77]. Studies have been conducted on porcine GGTA1 or gene knockout of GGTA1 and CMAH, which can reduce the generation of α-1, 3-Gal epitope [77]. Consequently, the potential utilization of pTDM for tooth root regeneration is worth considering.

5. Conclusion

In summary, this study compared the odontogenic differentiation-inducing ability of pTDM and hTDM *in vitro* and *in vivo,* and the two TDM scaffolds exhibited a similar odontogenesis-inducing ability. When compared to hTDM, the protein composition of pTDM revealed the presence of 58 coexisting proteins. The analysis revealed that evolutionarily conserved coexisting proteins in pTDM may confer an odontogenic capacity comparable to that of hTDM. These findings provide ideas for making full use of the porcine-derived ECM scaffold pTDM, which can address the scarcity of hTDM and facilitate the advancement of novel strategies for tooth tissue regeneration. Additionally, it provides innovative perspectives on mitigating the immune responses triggered by allogeneic and xenogeneic TDM.

Ethics approval and consent to participate

All experimental procedures were performed according to the ethical guidelines of the Helsinki Declaration and approved by Ethics Committee of College of Stomatology, Chongqing Medical University, Chongqing, China (CQHS-REC-2021 (LSNo.040)).

Funding

This study was supported by the National Natural Science Foundation of China [Grant No. 82071072], Program for Youth Innovation in Future Medicine, Chongqing Medical University [Grant No. W0179], and Scientific and Young and Middle-aged Senior Medical Talents studio of Chongqing [Grant No. ZQNYXGDRCGZS2019004].

CRediT authorship contribution statement

Xiya Zhang: Conceptualization, Investigation, Methodology, Writing – review & editing. **Sha Zhou:** Investigation, Methodology, Validation. **Yuzhen Zhan:** Investigation, Methodology, Writing – original draft. **Ziyi Mei:** Investigation, Validation. **Aizhuo Qian:** Investigation, Validation. **Yu Yuan:** Investigation, Validation. **Xiaonan Zhang:** Supervision. **Tiwei Fu:** Methodology. **Shiyong Ma:** Methodology, Visualization. **Jie Li:** Funding acquisition, Resources, Supervision.

Declaration of competing interest

The authors declare that they have no known competing financial interests or personal relationships that could have appeared to influence the work reported in this paper.

Data availability

Data will be made available on request.

Appendix A. Supplementary data

Supplementary data to this article can be found online at https://doi.org/10.1016/j.mtbio.2024.100990.

Abbreviations

TDM	treated dentin matrix
ECM	extracellular matrix
SHEDs	stem cells from human exfoliated deciduous teeth
3D	three-dimensional
DMP1	dentin matrix protein 1
DSPP	dentin sialophosphoprotein
DFCs	dental follicle cells
EDTA	ethylenediaminetetraacetic acid
PBS	phosphate-buffered saline
α-MEM	α-minimum essential medium
FBS	fetal bovine serum
SEM	scanning electron microscopy
H&E	hematoxylin-eosin
SDS-PAGE	sodium dodecyl sulfate-polyacrylamide gel electrophoresis
FASP	filter aided sample preparation
LC-MS	liquid chromatography-mass spectrometry
KEGG	kyoto encyclopedia of genes and genomes
GO	gene ontology
HA/TCP	biphasic hydroxyapatite/tricalcium phosphate

References

[1] A.D. Theocharis, S.S. Skandalis, C. Gialeli, N.K. Karamanos, Extracellular matrix structure, Advanced drug delivery reviews 97 (2016) 4–27.
[2] D. Wilhelm, H. Kempf, A. Bianchi, J.B. Vincourt, ATDC5 cells as a model of cartilage extracellular matrix neosynthesis, maturation and assembly, Journal of proteomics 219 (2020) 103718.
[3] K.M. Galler, F.P. Brandl, S. Kirchhof, M. Widbiller, A. Eidt, W. Buchalla, A. Göpferich, G. Schmalz, Suitability of different natural and synthetic biomaterials for dental pulp tissue engineering, Tissue engineering. Part A 24 (2018) 234–244.
[4] L. Tavelli, M.K. McGuire, G. Zucchelli, G. Rasperini, S.E. Feinberg, H.L. Wang, W. V. Giannobile, Extracellular matrix-based scaffolding technologies for periodontal and peri-implant soft tissue regeneration, Journal of periodontology 91 (2020) 17–25.
[5] D. Bejleri, M.E. Davis, Decellularized extracellular matrix materials for cardiac repair and regeneration, Advanced healthcare materials 8 (2019) e1801217.
[6] K.E. Benders, P.R. van Weeren, S.F. Badylak, D.B. Saris, W.J. Dhert, J. Malda, Extracellular matrix scaffolds for cartilage and bone regeneration, Trends in biotechnology 31 (2013) 169–176.
[7] P. Rousselle, M. Montmasson, C. Garnier, Extracellular matrix contribution to skin wound re-epithelialization, Matrix biology : journal of the International Society for Matrix Biology 75–76 (2019) 12–26.
[8] M. Grawish, L. Grawish, H. Grawish, M. Grawish, A. Holiel, N. Sultan, S. El-Negoly, Demineralized dentin matrix for dental and alveolar bone tissues regeneration: an innovative scope review, in: Tissue Engineering and Regenerative Medicine, vol. 19, 2022.
[9] S. Virdee, N. Bashir, J. Camilleri, P. Cooper, P. Tomson, Exploiting dentine matrix proteins in cell-free approaches for periradicular tissue engineering, Tissue Engineering Part B: Reviews 28 (2021).
[10] F. Bi, Z. Zhang, W. Guo, Treated dentin matrix in tissue regeneration: recent advances, Pharmaceutics 15 (2022) 91.
[11] S.F. Badylak, The extracellular matrix as a biologic scaffold material, Biomaterials 28 (2007) 3587–3593.
[12] K.E.M. Benders, P.R.v. Weeren, S.F. Badylak, D.B.F. Saris, W.J.A. Dhert, J. Malda, Extracellular matrix scaffolds for cartilage and bone regeneration, Trends in Biotechnology 31 (2013) 169–176.
[13] S. Liu, J. Sun, S. Yuan, Y. Yang, Y. Gong, Y. Wang, R. Guo, X. Zhang, Y. Liu, H. Mi, M. Wang, M. Liu, R. Li, Treated dentin matrix induces odontogenic differentiation of dental pulp stem cells via regulation of Wnt/β-catenin signaling, Bioactive materials 7 (2022) 85–97.
[14] X. Yang, Y. Ma, W. Guo, B. Yang, W. Tian, Stem cells from human exfoliated deciduous teeth as an alternative cell source in bio-root regeneration, Theranostics 9 (2019) 2694–2711.
[15] B. Yang, G. Chen, J. Li, Q. Zou, D. Xie, Y. Chen, H. Wang, X. Zheng, J. Long, W. Tang, W. Guo, W. Tian, Tooth root regeneration using dental follicle cell sheets in combination with a dentin matrix - based scaffold, Biomaterials 33 (2012) 2449–2461.
[16] R. Li, W. Guo, B. Yang, L. Guo, L. Sheng, G. Chen, Y. Li, Q. Zou, D. Xie, X. An, Y. Chen, W. Tian, Human treated dentin matrix as a natural scaffold for complete human dentin tissue regeneration, Biomaterials 32 (2011) 4525–4538.
[17] W. Guo, Y. He, X. Zhang, W. Lu, C. Wang, H. Yu, Y. Liu, Y. Li, Y. Zhou, J. Zhou, M. Zhang, Z. Deng, Y. Jin, The use of dentin matrix scaffold and dental follicle cells for dentin regeneration, Biomaterials 30 (2009) 6708–6723.
[18] W. Guo, K. Gong, H. Shi, G. Zhu, Y. He, B. Ding, L. Wen, Y. Jin, Dental follicle cells and treated dentin matrix scaffold for tissue engineering the tooth root, Biomaterials 33 (2012) 1291–1302.
[19] J. Sun, J. Li, H. Li, H. Yang, J. Chen, B. Yang, F. Huo, W. Guo, W. Tian, tBHQ suppresses osteoclastic resorption in xenogeneic-treated dentin matrix-based scaffolds, Advanced healthcare materials 6 (2017).
[20] H. Li, J. Sun, J. Li, H. Yang, X. Luo, J. Chen, L. Xie, F. Huo, T. Zhu, W. Guo, W. Tian, Xenogeneic bio-root prompts the constructive process characterized by macrophage phenotype polarization in rodents and nonhuman primates, Advanced healthcare materials 6 (2017).
[21] X. Luo, B. Yang, L. Sheng, J. Chen, H. Li, L. Xie, G. Chen, M. Yu, W. Guo, W. Tian, CAD based design sensitivity analysis and shape optimization of scaffolds for bio-root regeneration in swine, Biomaterials 57 (2015) 59–72.
[22] H. Li, B. Ma, H. Yang, J. Qiao, W. Tian, R. Yu, Xenogeneic dentin matrix as a scaffold for biomineralization and induced odontogenesis, Biomedical materials (Bristol, England) 16 (2021).
[23] T. Sutherland, D. Dyer, J. Allen, The extracellular matrix and the immune system: a mutually dependent relationship, Science (New York, N.Y.) 379 (2023) eabp8964.
[24] H. Yang, J. Li, Y. Hu, J. Sun, W. Guo, H. Li, J. Chen, F. Huo, W. Tian, S. Li, Treated dentin matrix particles combined with dental follicle cell sheet stimulate periodontal regeneration, Dental materials: official publication of the Academy of Dental Materials 35 (2019) 1238–1253.
[25] D.K.C. Cooper, R. Gaston, D. Eckhoff, J. Ladowski, T. Yamamoto, L. Wang, H. Iwase, H. Hara, M. Tector, A.J. Tector, Xenotransplantation-the current status and prospects, British medical bulletin 125 (2018) 5–14.
[26] D. Niu, X. Ma, T. Yuan, Y. Niu, Y. Xu, Z. Sun, Y. Ping, W. Li, J. Zhang, T. Wang, G. M. Church, Porcine genome engineering for xenotransplantation, Advanced drug delivery reviews 168 (2021) 229–245.
[27] Y. Yuan, X. Zhang, Y. Zhan, S. Tang, P. Deng, Z. Wang, J. Li, Adipose-derived stromal/stem cells are verified to be potential seed candidates for bio-root regeneration in three-dimensional culture, Stem cell research & therapy 13 (2022) 234.
[28] J. Li, H. Yang, Q. Lu, D. Chen, M. Zhou, Y. Kuang, S. Ying, J. Song, Proteomics and N-glycoproteomics analysis of an extracellular matrix-based scaffold-human treated dentin matrix, Journal of tissue engineering and regenerative medicine 13 (2019) 1164–1177.
[29] S. Maere, K. Heymans, M. Kuiper, BiNGO: a Cytoscape plugin to assess overrepresentation of gene ontology categories in biological networks, Bioinformatics (Oxford, England) 21 (2005) 3448–3449.
[30] R.C. Edgar, MUSCLE: multiple sequence alignment with high accuracy and high throughput, Nucleic acids research 32 (2004) 1792–1797.
[31] I. Letunic, P. Bork, Interactive Tree of Life (iTOL) v4: recent updates and new developments, Nucleic acids research 47 (2019) W256–w259.

[32] N. Xiao, D.S. Cao, M.F. Zhu, Q.S. Xu, protr/ProtrWeb: R package and web server for generating various numerical representation schemes of protein sequences, Bioinformatics (Oxford, England) 31 (2015) 1857–1859.
[33] T. Muetze, I.H. Goenawan, H.L. Wiencko, M. Bernal-Llinares, K. Bryan, D.J. Lynn, Contextual Hub Analysis Tool (CHAT): a Cytoscape app for identifying contextually relevant hubs in biological networks, F1000Research 5 (2016) 1745.
[34] N. Maillet, Rapid Peptides Generator: fast and efficient in silico protein digestion, NAR genomics and bioinformatics 2 (2020) lqz004.
[35] Y. Zhu, R. Zhu, J. Ma, Z. Weng, Y. Wang, X. Shi, Y. Li, X. Yan, Z. Dong, J. Xu, C. Tang, L. Jin, In vitro cell proliferation evaluation of porous nano-zirconia scaffolds with different porosity for bone tissue engineering, Biomedical materials (Bristol, England) 10 (2015) 055009.
[36] A.L. Krause, D. Beliaev, R.A. Van Gorder, S.L. Waters, Lattice and continuum modelling of a bioactive porous tissue scaffold, Mathematical medicine and biology : a journal of the IMA 36 (2019) 325–360.
[37] R. Garimella, X. Bi, H.C. Anderson, N.P. Camacho, Nature of phosphate substrate as a major determinant of mineral type formed in matrix vesicle-mediated in vitro mineralization: an FTIR imaging study, Bone 38 (2006) 811–817.
[38] R. Du, T. Wu, W. Liu, L. Li, L. Jiang, W. Peng, J. Chang, Y. Zhu, Role of the extracellular signal-regulated kinase 1/2 pathway in driving tricalcium silicate-induced proliferation and biomineralization of human dental pulp cells in vitro, Journal of endodontics 39 (2013) 1023–1029.
[39] H. Maeda, N. Wada, A. Tomokiyo, S. Monnouchi, A. Akamine, Prospective potency of TGF-β1 on maintenance and regeneration of periodontal tissue, International review of cell and molecular biology 304 (2013) 283–367.
[40] Y. Yamakoshi, S. Kinoshita, L. Izuhara, T. Karakida, M. Fukae, S. Oida, DPP and DSP are necessary for maintaining TGF-β1 activity in dentin, Journal of dental research 93 (2014) 671–677.
[41] G.S. Stein, J.B. Lian, Molecular mechanisms mediating proliferation/differentiation interrelationships during progressive development of the osteoblast phenotype, Endocrine reviews 14 (1993) 424–442.
[42] T. Sreenath, T. Thyagarajan, B. Hall, G. Longenecker, R. D'Souza, S. Hong, J. T. Wright, M. MacDougall, J. Sauk, A.B. Kulkarni, Dentin sialophosphoprotein knockout mouse teeth display widened predentin zone and develop defective dentin mineralization similar to human dentinogenesis imperfecta type III, The Journal of biological chemistry 278 (2003) 24874–24880.
[43] N. Linscheid, A. Santos, P.C. Poulsen, R.W. Mills, K. Calloe, U. Leurs, J.Z. Ye, C. Stolte, M.B. Thomsen, B.H. Bentzen, P.R. Lundegaard, M.S. Olesen, L.J. Jensen, J.V. Olsen, A. Lundby, Quantitative proteome comparison of human hearts with those of model organisms, PLoS biology 19 (2021) e3001144.
[44] H.D. Dawson, C. Chen, B. Gaynor, J. Shao, J.F. Urban Jr., The porcine translational research database: a manually curated, genomics and proteomics-based research resource, BMC genomics 18 (2017) 643.
[45] P. Zhang, X. Liu, P. Guo, X. Li, Z. He, Z. Li, M.J. Stoddart, S. Grad, W. Tian, D. Chen, X. Zou, Z. Zhou, S. Liu, Effect of cyclic mechanical loading on immunoinflammatory microenvironment in biofabricating hydroxyapatite scaffold for bone regeneration, Bioactive materials 6 (2021) 3097–3108.
[46] J. Caballé-Serrano, M. Fujioka-Kobayashi, D.D. Bosshardt, R. Gruber, D. Buser, R. J. Miron, Pre-coating deproteinized bovine bone mineral (DBBM) with bone-conditioned medium (BCM) improves osteoblast migration, adhesion, and differentiation in vitro, Clinical oral investigations 20 (2016) 2507–2513.
[47] F. Faot, S. Deprez, K. Vandamme, G.V. Camargos, N. Pinto, J. Wouters, J. van den Oord, M. Quirynen, J. Duyck, The effect of L-PRF membranes on bone healing in rabbit tibiae bone defects: micro-CT and biomarker results, Scientific reports 7 (2017) 46452.
[48] J.S. Lee, G. Mitulović, L. Panahipour, R. Gruber, Proteomic analysis of porcine-derived collagen membrane and matrix, Materials (Basel, Switzerland) 13 (2020).
[49] A.S. Goustin, A.B. Abou-Samra, The "thrifty" gene encoding Ahsg/Fetuin-A meets the insulin receptor: insights into the mechanism of insulin resistance, Cell Signal 23 (2011) 980–990.
[50] P. Zilm, P. Bartold, Proteomic identification of proteinase inhibitors in the porcine enamel matrix derivative, EMD (R), Journal of periodontal research 46 (2011) 111–117.
[51] A. Dabrowska, J. Tarach, B. Wojtysiak-Duma, D. Duma, Fetuin-A (AHSG) and its usefulness in clinical practice, in: Review of the Literature, Biomedical papers of the Medical Faculty of the University Palacky, Olomouc, 2015. *Czechoslovakia* **159**.
[52] K. Mori, M. Emoto, M. Inaba, Fetuin-A: a multifunctional protein, Recent patents on endocrine, metabolic & immune drug discovery 5 (2011) 124–146.
[53] L. Brylka, W. Jahnen-Dechent, The role of fetuin-A in physiological and pathological mineralization, Calcified tissue international 93 (2013).
[54] Y. Takagi, J. Kindaichi, K. Moriyama, M. Suzuki, H. Shimokawa, S. Sasaki, Distribution of α2Hs glycoprotein in pathological human dentins 30 (2009) 309–321.
[55] J. Fitzgerald, J. Bateman, A new FACIT of the collagen family: COL21A1 1 1 the collagen 21 DNA (and protein) sequence has been deposited in GenBank (accession number AF414088), Febs Letters - FEBS LETT 505 (2001) 275–280.
[56] G. Lisignoli, K. Codeluppi, K. Todoerti, C. Manferdini, A. Piacentini, N. Zini, F. Grassi, L. Cattini, R. Piva, V. Rizzoli, A. Facchini, N. Giuliani, A. Neri, Gene array profile identifies collagen type XV as a novel human osteoblast-secreted matrix protein, Journal of cellular physiology 220 (2009) 401–409.
[57] K.-L. Chen, Y.-Y. Huang, J. Lung, Y.-Y. Yeh, K. Yuan, CD44 is involved in mineralization of dental pulp cells, Journal of endodontics 39 (2013) 351–356.
[58] C. Bal, N. Oztas, M. Cincik, E. Barış, Immunolocalization of fibronectin during reparative dentinogenesis in rat molor teeth after pulp capping with mineral trioxide aggregate or calcium hydroxide, The New York state dental journal 77 (2011) 36–42.
[59] K. Nagasaki, M. Chavez, A. Nagasaki, J. Taylor, M. Tan, M. Ma, E. Ralston, M. Thew, D.G. Kim, M. Somerman, B. Foster, The bone sialoprotein RGD domain modulates and maintains periodontal development, Journal of dental research 101 (2022) 220345221100794.
[60] H.S. Shapiro, H.S. Shapiro, J. Chen, J.L. Wrana, J.L. Wrana, Q. Zhang, M. Blum, J. Sodek, J. Sodek, Characterization of porcine bone sialoprotein: primary structure and cellular expression, Matrix 13 (6) (1993) 431–440.
[61] J. Chen, K. Sasaguri, J. Sodek, J. Sodek, T.B. Aufdemorte, H. Jiang, H.F. Thomas, Enamel epithelium expresses bone sialoprotein (BSP), European journal of oral sciences 106 (Suppl 1) (1998) 331–336.
[62] A. Gullard, J. Gluhak-Heinrich, S. Papagerakis, P. Sohn, A. Unterbrink, S. Chen, M. Macdougall, MEPE localization in the craniofacial complex and function in tooth dentin formation, Journal of Histochemistry & Cytochemistry 64 (2016).
[63] L. Merametdjian, S. Beck-Cormier, N. Bon, G. Couasnay, S. Sourice, J. Guicheux, C. Gaucher, L. Beck, Expression of phosphate transporters during dental mineralization, Journal of Dental Research 97 (2017) 002203451772981.
[64] H. Chen, Z. Huang, C. Chen, The role of histone acetylation modification in dental tissue-derived mesenchymal stem cells and odontogenesis, Cellular reprogramming 25 (2022).
[65] J. Li, S. Diao, H. Yang, Y. Cao, J. Du, D. Yang, IGFBP5 promotes angiogenic and neurogenic differentiation potential of dental pulp stem cells, Development, Growth & Differentiation 61 (2019).
[66] K. Fjeld, P. Kettunen, T. Furmanek, I. Kvinnsland, K. Luukko, Dynamic Expression of Wnt Signaling-Related Dickkopf1, -2, and -3 mRNAs in the Developing Mouse Tooth, vol. 233, Developmental dynamics : an official publication of the American Association of Anatomists, 2005, pp. 161–166.
[67] T. Niwa, Y. Yamakoshi, H. Yamazaki, T. Karakida, R. Chiba, J.C. Hu, T. Nagano, R. Yamamoto, J.P. Simmer, H.C. Margolis, K. Gomi, The dynamics of TGF-β in dental pulp, odontoblasts and dentin, Scientific reports 8 (2018) 4450.
[68] H. Bismar, T. Klöppinger, E.M. Schuster, S. Balbach, I. Diel, R. Ziegler, J. Pfeilschifter, Transforming growth factor beta (TGF-beta) levels in the conditioned media of human bone cells: relationship to donor age, bone volume, and concentration of TGF-beta in human bone matrix in vivo, Bone 24 (1999) 565–569.
[69] B. Hoac, M. Østergaard, N.K. Wittig, T. Boukpessi, D.J. Buss, C. Chaussain, H. Birkedal, M. Murshed, M.D. McKee, Genetic ablation of osteopontin in osteomalacic hyp mice partially rescues the deficient mineralization without correcting hypophosphatemia, Journal of bone and mineral research : the official journal of the American Society for Bone and Mineral Research 35 (2020) 2032–2048.
[70] L. Wang, B.L. Foster, V. Kram, F.H. Nociti Jr., P.M. Zerfas, A.B. Tran, M.F. Young, M.J. Somerman, Fibromodulin and biglycan modulate periodontium through TGFβ/BMP signaling, Journal of dental research 93 (2014) 780–787.
[71] Y. Shi, Y. Yu, Y. Zhou, J. Zhao, W. Zhang, D. Zou, W. Song, S. Wang, A single-cell interactome of human tooth germ from growing third molar elucidates signaling networks regulating dental development, Cell & bioscience 11 (2021) 178.
[72] X. Yuan, M. Liu, X. Cao, S. Yang, Ciliary IFT80 regulates dental pulp stem cells differentiation by FGF/FGFR1 and Hh/BMP2 signaling, International journal of biological sciences 15 (2019) 2087–2099.
[73] T.R. St Amand, Y. Zhang, E.V. Semina, X. Zhao, Y. Hu, L. Nguyen, J.C. Murray, Y. Chen, Antagonistic signals between BMP4 and FGF8 define the expression of Pitx1 and Pitx2 in mouse tooth-forming anlage, Developmental biology 217 (2000) 323–332.
[74] A.C. Shirali, D.R. Goldstein, Activation of the innate immune system by the endogenous ligand hyaluronan, Current opinion in organ transplantation 13 (2008) 20–25.
[75] H. Zhou, H. Hara, D.K.C. Cooper, The complex functioning of the complement system in xenotransplantation, Xenotransplantation 26 (2019) e12517.
[76] Y. Zhang, Q. Liu, S. Yang, Q. Liao, CD58 immunobiology at a glance, Frontiers in immunology 12 (2021) 705260.
[77] H. Tritschler, K. Fischer, J. Seissler, J. Fiedler, R. Halbgebauer, M. Huber-Lang, A. Schnieke, R.E. Brenner, New insights into xenotransplantation for cartilage repair: porcine multi-genetically modified chondrocytes as a promising cell source, Cells 10 (2021).